Mineralization from Aqueous Solutions of Zinc Salts Directed by Amino Acids and Peptides

Peter Gerstel,[†] Rudolf C. Hoffmann,*[,†] Peter Lipowsky,[†] Lars P. H. Jeurgens,[‡] Joachim Bill,[†] and Fritz Aldinger[†]

Pulvermetallurgisches Laboratorium, Max-Planck-Institut für Metallforschung and Institut für Nichtmetallische Anorganische Materialien, Universität Stuttgart, Pulvermetallurgisches Laboratorium, Heisenbergstr. 3, D-70569 Stuttgart, Germany, and Max-Planck-Institut für Metallforschung, Department Mittemeijer, Stuttgart, Germany

Received July 15, 2005. Revised Manuscript Received October 28, 2005

The suitability of amino acids and dipeptides as structure-directing agents for the deposition of coatings from aqueous solutions of zinc salts is discussed. According to a bio-inspired approach, the influence of these biomolecules was investigated with respect to the evolution of architectures based on zinc oxide and basic zinc salts. The small molecules were able to trigger the morphology of these materials ranging from grainlike to two-dimensional up to three-dimensional features. Besides morphological aspects, the structural characterization of these solids by means of electron and atomic force microscopies, photoelectron and infrared spectroscopies, and X-ray diffraction are discussed in order to extract the function of the biomolecules with regard to the formation of the inorganic phases.

Introduction

Zinc oxide and zinc oxide based materials or devices are promising candidates for several functional applications such as UV light emitters, gas sensors, and acoustic wave devices, which accounts for many attempts at miniaturization and nanostructuring.[1,2] As an alternative and complement to conventional routes for the deposition of thin films, the method of chemical bath deposition (CBD) was introduced.[3] CBD here refers to the thermohydrolysis (or "forced hydrolysis") of metal salts for the fabrication of oxidic films. However, in the case of zinc oxide the deposition behavior is strongly influenced by the tendency to form elongated micron-long crystals (sometimes termed "nanorods") that have made the formation of smooth homogeneous nanostructures so far impossible.[3,4] Recently, the preparation of zinc oxide based nanostructured films without these insufficiencies was reported.[5,6] The method applied involves macromolecular organic additives such as graft copolymers[5] or homopolymers,[6] which are added to the deposition medium. Owing to the interaction of these polymers with zinc oxide in solution, the growth of micron-size crystals is suppressed and organic/inorganic hybrid nanoparticles are formed within the deposition solution. The subsequent assembly of these particles can be controlled by organically modified surfaces and yields nanostructured films with luminescent properties.[6]

The interaction of organic molecules with inorganic phases is also observed in living nature, e.g., in the case of biomineralization processes that lead to the formation of complex organic/inorganic structures.[7] Furthermore, there are examples where metal ions interact with bioorganic molecules. In this connection, amino acids such as histidine are involved, e.g., within the so-called zinc finger, a configuration of a DNA-binding protein.[8] Accordingly, a large number of zinc complexes with amino acid ligands were investigated,[9] which might be suitable starting materials for solid-state structures.

In the present paper the hydrolysis of zinc salts in the presence of amino acids and dipeptides is investigated, whereby the suitability of such organic molecules as structure-directing agents is revealed. The main aim was to demonstrate that this bio-inspired approach provides a means for the deposition of a variety of morphologies ranging from grainlike to two-dimensional up to three-dimensional features.

Experimental Section

Substrate Preparation. Substrates consisted of surface-oxidized silicon, whereby further modification with layer-by-layer assemblies (LBLs) of polyelectrolytes was also employed. Deposition experiments were carried out on both types of surfaces.

* To whom correspondence should be addressed. E-mail: hoffmann@mf.mpg.de.

[†] Max-Planck-Institut für Metallforschung and Institut für Nichtmetallische Anorganische Materialien.

[‡] Max-Planck-Institut für Metallforschung, Department Mittemeijer.

(1) Pearton, S. J.; Norton, D. P.; Ip, K.; Heo, Y. W.; Steiner, T. *Superlattices Microstruct.* **2003**, *34*, 3.
(2) Wang, Z. L. *J. Phys.: Condens. Matter* **2004**, *16*, R829.
(3) Bill, J.; Hoffmann, R. C.; Fuchs, T. M.; Aldinger, F. *Z. Metallkd.* **2002**, *93*, 478.
(4) Hoffmann, R. C.; Jia, S.; Bill, J.; De Guire, M. R.; Aldinger, F. *J. Ceram. Soc. Jpn.* **2004**, *112−1*, S1089.
(5) Hoffmann, R. C.; Jia, S.; Bartolomé, J. C.; Fuchs, T. M.; Bill, J.; Graat, P. C. J.; Aldinger, F. *J. Eur. Ceram. Soc.* **2003**, *23*, 2119.
(6) Hoffmann, R. C.; Jia, S.; Jeurgens, L. P. H.; Bill, J.; Aldinger, F. *Mater. Sci. Eng., C: Biomimetic Supramol. Syst.* (in press).
(7) See, e.g.: Mann, S. *Biomineralization*; Oxford Chemistry Masters; Oxford University Press: Oxford, 2001.
(8) See, e.g.: Lippard, S. J.; Berg, J. M. *Principles of Bioinorganic Chemistry*; University Science Books: Mill Valley, CA, 1994; pp 178−183.
(9) Rombach, M.; Gelinsky, M.; Vahrenkamp, H. *Inorg. Chim. Acta* **2002**, *334*, 25.

10.1021/cm051542o CCC: $33.50
Published on Web 12/10/2005

Silicon wafers were cleaned and surface oxidized in Piranha solution [concentrated H_2SO_4:H_2O_2 (30 wt % in water) = 70:30, v:v], washed abundantly with distilled water, and dried in an argon stream prior to use. LBLs of polyelectrolytes were prepared, if applied in the deposition experiment, by dipping the silicon wafer in an aqueous 0.5 wt % solution of the desired polyelectrolyte for 20 min, followed by immersion in distilled water for 5 min. Subsequent layers were obtained without intermediate drying between the immersions in oppositely charged polyelectrolytes according to published procedures.[10] Aqueous polyelectrolyte solutions were obtained from commercially available products by dilution with water (poly(ethyleneimine), PEI (Aldrich, M_w 70 000); poly(sodium 4-styrenesulfonate), PS (Aldrich, M_w 70 000); and poly(allylamine hydrochloride), PAH (Aldrich, M_w 70 000)). The pH of the PEI solution was adjusted to 3 with hydrochloric acid; PS and PAH solutions were used without further conditioning. All LBLs in this work had the sequence (PEI/PSS)(PAH/PSS)7.

Deposition Experiments. Several series of deposition experiments were carried out with zinc nitrate and hexamethylenetetramine (HMTA) concentrations in the reaction solution of either 15 or 30 mM, respectively, with a constant ratio of [Zn]:[HMTA] of 1:1 but varying ratios of amino acids or dipeptides. The stereo configuration of all amino acids including those in dipeptides was L in all cases. To ensure optically clear starting solutions, all compounds were mixed always freshly prior to use. Therefore, amino acids or peptides were dissolved in an HMTA stock solution and mixed with according volumes of a zinc nitrate solution to obtain the above-mentioned concentrations.

Substrates were immersed in 2 mL aliquots of the reaction solution at 343 K until the onset of visible turbidity in the case of His and Gly-His. Longer reaction times did not lead to significantly thicker films and larger agglomerates from the solution sedimented on the substrate. In the case of [Zn] = 15 mM turbidity was observed after 4.5 h for [Zn]:[His] = 1:1, 5.5 h for [Zn]:[His] = 2:1, 6.5 for [Zn]:[His] = 4:1, and 3.5 h for [Zn]:[Gly-His] = 2:1, respectively. In the case of [Zn]:[His] = 8:1 no turbidity was observed until the termination of the reaction after 6.75 h. Depositions with all other amino acids or peptides were carried out for 48 h at 333 K.

For comparison of the before-mentioned films from solutions containing His with a reference substance, $Zn(His)_2$ powder was synthesized[11] and compacted to pellets.

Film Characterization. *X-ray Photoelectron Spectroscopy (XPS).* XPS analysis was performed with a Thermo VG Thetaprobe 300 system using monochromatic incident Al Kα radiation ($h\nu$ = 1486.68 eV; spot size 400 μm; base pressure $<10^{-7}$ Pa; average detection angle of 53° with respect to the sample surface). Energy calibration, removal of contaminants, and charge compensation during the measurements were carried out according to established procedures.[12] Spectral decomposition of the as-measured spectra was performed by subtraction of a Shirley-type inelastic background over the concerned binding energy (BE) range for each spectral region, and subsequent, constrained, linear-least-squares fitting with one or more symmetric (mixed Gaussian−Lorentzian) peak components (while taking the same Gaussian−Lorentzian fraction and full width at half-maximum (fwhm) for each component in the fitted spectrum). Finally, the BE scales for each set of resolved Zn 2p were aligned by shifting the spectra according to the difference between the resolved, lowest-BE oxidic Zn $2p_{3/2}$ main peak and the corresponding reference value of 1021.9 ± 0.1 eV for pure ZnO,[13] whereby this approach also led to reasonable values for the accordingly shifted set of O 1s, N 1s, and C 1s signals. In the spectra recorded from the $Zn(His)_2$ reference, the oxidic Zn $2p_{3/2}$ peak corresponding to the chemical environment of Zn in ZnO is absent and the alignment of the BE scales was done by shifting the resolved Zn $2p_{3/2}$ main peak to the value of 1027.8 ± 0.1 eV as determined above. This approach also led to reasonable values for the binding energies of the lighter elements, and the contributions to the C 1s, O 1s, and N 1s peaks could be determined in a curve-fitting procedure.

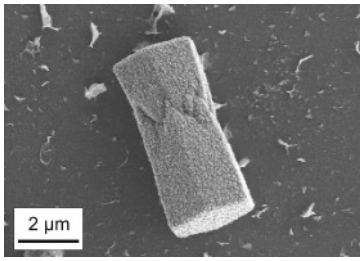

Figure 1. SEM micrograph of zincite from solutions containing 30 mM [Zn], 30 mM HMTA, and 3.75 mM Pro.

Atomic Force Microscopy (AFM). Images were recorded using a Digital Instruments Nanoscope III applying tapping mode with silicon cantilevers.

Scanning Electron Microscopy (SEM). Micrographs were taken with a Zeiss DSM 982 Gemini at 1.7 kV or a JEOL 6300F at 2 kV.

X-ray Diffraction (XRD). Diagrams were measured with a Siemens D5000 Kristalloflex diffractometer in Bragg−Brentano geometry using Cu $K\alpha_1$ radition.

Infrared Spectroscopy (IR). Samples were obtained by collecting deposition products from several wafers, mixing with KBr, and compaction to pellets. Transmission spectra were measured using a Nicolet Avatar 360.

Zeta-Potential Measurements. A Zetasizer Malvern 3000 HSA was used to measure the electrophoretic mobility. Measurements were carried out for reaction solutions from 30 mM [Zn], 30 mM HMTA, and 30 mM His after the onset of turbidity, which showed a potential of +22.0 mV at pH 6.7. To improve the reliability, a series of three separate measurements (298 K) was collected.

Results and Discussion

The addition of glycyl-glutamine (Gly-Gln), citrulline (Cit), and proline (Pro) led to the formation of micrometer-size crystals, presumably multiple twins of zincite (Figure 1). Such twinning of zincite was found to be typical for precipitation in the presence of additives containing carboxylate functions.[14] A control experiment without the addition of biomolecules, though, yielded a similar precipitate consisting of hexagonal crystals of zincite. This might indicate a rather weak interaction of the above-mentioned amino acids and dipeptides with the mineralization product in comparison to the other employed additives.

In the presence of histidine (His) or glycyl-histidine (Gly-His) films were formed, whereby SEM micrographs revealed a complete and uniform surface coverage for low [Zn]:[His]

(10) Decher, G. *Science* **1997**, *277*, 1232.
(11) Weitzel, G.; Schneider, F.; Frentzdorff, A.; Heyke, H. *Z. Physiol. Chem.* **1957**, *307*, 14.
(12) Hoffmann, R. C.; Jeurgens, L. P. H.; Wildhack, S.; Bill, J.; Aldinger, F. *Chem. Mater.* **2004**, *16*, 4199.
(13) Wagner, C. D.; Riggs, W. M.; Davis, L. E.; Moulder, J. F.; Muilenberg, G. E.; *Handbook of X-ray Photoelectron Spectroscopy*; Perkin-Elmer Corporation, Physical Electronics Division: Eden Prairie, MN, 1979.
(14) Öner, M.; Norwig, J.; Meyer, W. H.; Wegner, G. *Chem. Mater.* **1998**, *10*, 460.

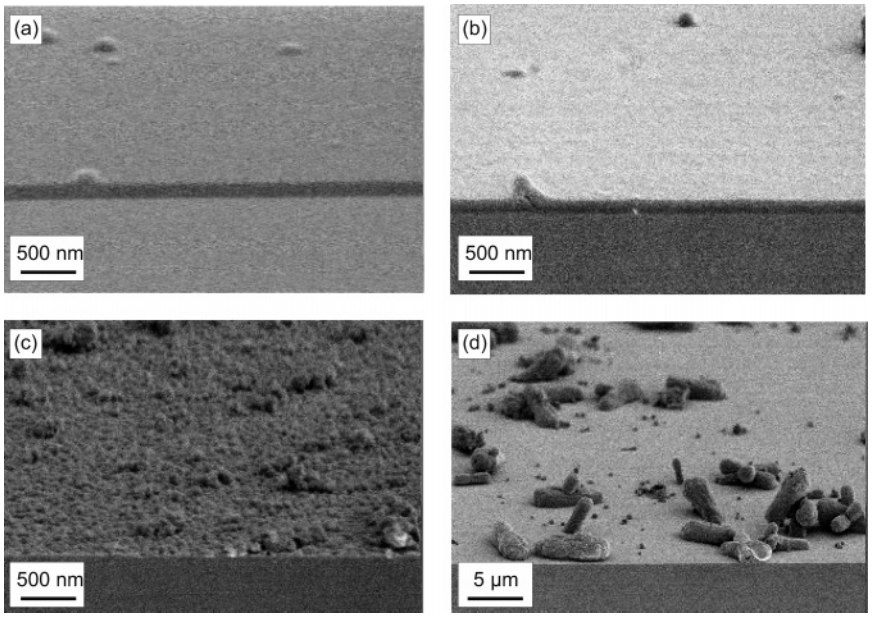

Figure 2. SEM micrographs of as-deposited films grown on silicon from solutions containing 15 mM [Zn], 15 mM HMTA, and various amounts of His at 343 K (reaction time): (a) [Zn]:[His] = 1:1 (4.5 h), (b) [Zn]:[His] = 2:1 (5.5 h), (c) [Zn]:[His] = 4:1 (6.5 h), and (d) [Zn]:[His] = 8:1 (6.75 h).

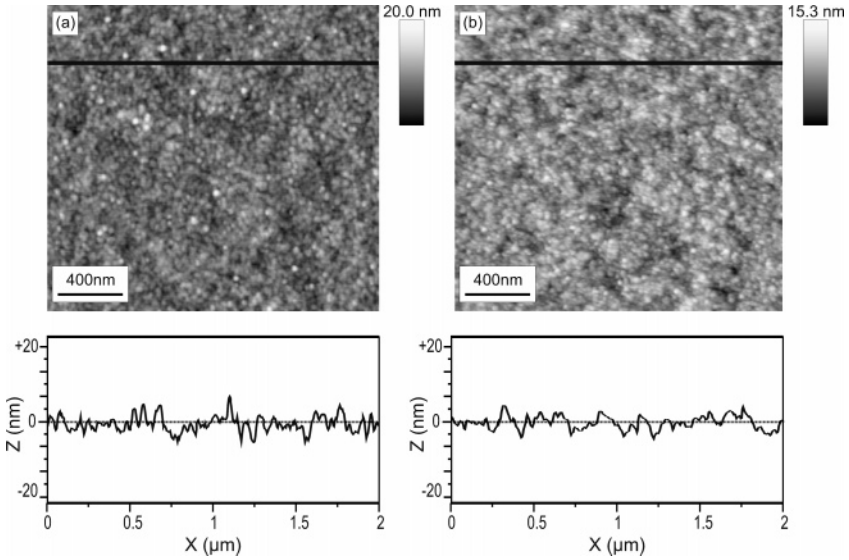

Figure 3. AFM images and cross sections of as-deposited films grown on silicon from solutions containing 15 mM [Zn], 15 mM HMTA, and various amounts of His at 343 K: (a) [Zn]:[His] = 1:1 (RMS 2.0 nm), (b) [Zn]:[His] = 2:1 (RMS 1.7 nm). The reaction conditions correspond to the samples in Figure 2a,b.

ratios (Figure 2a−c). Below a threshold concentration of His, though, the deposition of larger colloids instead of film formation was observed (Figure 2d). The cross sections of the interference colored films exhibited a thickness between 160 (Figure 2a), 140 (Figure 2b), and 50 nm (Figure 2c). As indicated by these SEM investigations and moreover according to AFM measurements, the ratio of roughness to thickness of the films increased with higher [Zn]:[His] ratios (Figure 3), suggesting that the presence of histidine minimizes the tendency of zinc oxide to form larger, elongated crystals. This corresponds to earlier investigations in which graft copolymers were used to inhibit the growth of zincite microcrystals and stabilize nanoparticles for uniform film growth.[3,4]

XPS was applied to investigate the effect of organic additives His and Gly-His in the reaction solution on the chemical constitution of the resulting thin films (Figures 4 and 5). To this end, detailed spectra of the Zn 2p, O 1s, N 1s, and C 1s photoelectron lines, as well as survey spectra over a wide BE range from 0 to 1400 eV, were recorded for films obtained from reaction solutions containing His and Gly-His. To establish the chemical states of the constituent atoms in the oxide products, the different spectral components constituting the measured Zn $2p_{3/2}$, C 1s, O 1s, and N 1s spectra were resolved by constrained peak fitting. The BE values of the thus resolved peak components are reported in Tables 1 and 2. For all cases studied, the XPS analysis indicated the presence of Zn, C, O, and N within the formed products (for an example, see Figure 4), thereby confirming the incorporation of amino acids in the films for all cases studied.

The measured Zn $2p_{3/2}$ spectra could be accurately fitted with up to four different peak components (Figure 5). The resolved Zn $2p_{3/2}$ peak positioned at the lowest BE of 1021.9

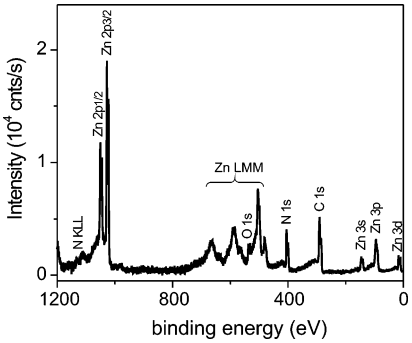

Figure 4. XPS spectrum (after charge correction and subtraction of a universal Tougaard background) recorded from an as-deposited oxide film grown on silicon from a solution containing 15 mM [Zn], 15 mM HMTA, and 15 mM His. The different photoelectron and Auger lines originating from the various oxide-film constituents are indicated.

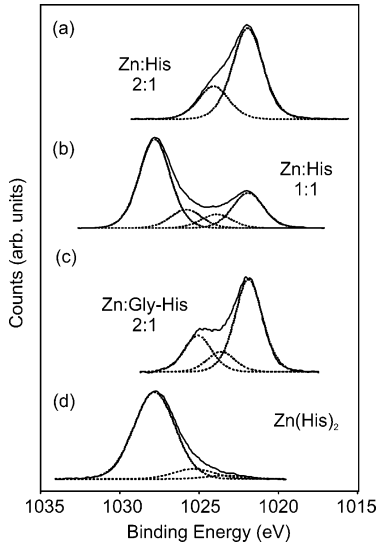

Figure 5. XPS spectra of as-deposited films from solutions containing (a) 15 mM [Zn], 15 mM HMTA, and 7.5 mM His; (b) 15 mM [Zn], 15 mM HMTA, and 15 mM His; and (c) 15 mM [Zn], 15 mM HMTA, and 7.5 mM Gly-His. (d) Spectrum of the $Zn(His)_2$ reference for comparison.

Table 1. Binding Energies (BE; in eV) of Zn $2p_{3/2}$ Peak Components as Resolved by Constrained Peak Fitting of Charge-Corrected XPS Spectra of the Prepared Oxide Films[a]

additive	Zn $2p_{3/2}$ BE (eV)			
(a) Zn:His 2:1	1021.9	1024.1		
(b) Zn:His 1:1	1021.9	1023.9	1025.8	1027.8
(c) Zn:Gly-His 2:1	1021.9	1023.6	1025.1	
(d) $Zn(His)_2$		1023.3	1025.4	1027.8

[a] The estimated error in the determination of the BE positions is about 0.2 eV.

Table 2. Binding Energies (BE; in eV) of the C 1s, O 1s, and N 1s Peak Components (Corresponding to the resolved Zn $2p_{3/2}$ Peak Components in Table 1) as Resolved by Constrained Peak Fitting of Charge-Corrected XPS Spectra of the Prepared Oxide Films[a]

additive	C 1s BE (eV)			O 1s BE (eV)			N 1s BE (eV)		
(a) Zn:His 2:1	284.7	287.0		531.5	533.7		398.9	401.1	
(b) Zn:His 1:1	285.3		290.5	531.2	534.0	537.2	399.0	402.3	404.8
(c) Zn:Gly-His 2:1	284.6	286.7	288.7	531.6	534.7		399.0	401.8	
(d) $Zn(His)_2$			290.6		534.5	537.7		402.1	404.7

[a] The estimated error in the determination of the BE positions is about 0.2 eV.

$\pm$ 0.1 eV corresponds to Zn in crystalline ZnO (Figure 5a–c; see also ref 13). After comparison with the corresponding $Zn(His)_2$ reference spectrum (compare Figure 5b with Figure 5d), the resolved Zn $2p_{3/2}$ peak component at the highest BE position of 1027.8 $\pm$ 0.2 eV could be identified with the local chemical environment for Zn atoms in the mononuclear complex $Zn(His)_2$ (as characterized by Zn atoms tetrahedrally surrounded by the oxygen atoms of two carboxylate groups[11,15]). This BE value of 1027.8 $\pm$ 0.2 eV can be compared with the corresponding BE value of 1027.0 eV, as reported for zinc acetate.[16] As reflected by comparison of Figure 5a,b, an increasing His concentration in the reaction solution results in a relative increase of Zn atoms being incorporated as $Zn(His)_2$ in the developing oxide film. Accordingly, a decrease of the His concentration results in an increasing contribution of ZnO to the reaction product. In addition to the two aforementioned main components, up to two relatively weaker components with intermediate BE values of 1025.5 $\pm$ 0.4 eV and 1023.6 $\pm$ 0.5 eV (i.e., between that for Zn in ZnO and Zn in $Zn(His)_2$; see Table 1) were resolved from the measured Zn $2p_{3/2}$ spectra. These components were less well-defined, which indicated the presence of Zn ions in a mixed environment.

Other amino acids or peptides, which were investigated for use as additives, led to more complex morphologies. The addition of tryptophyl-glycine (Trp-Gly) caused the formation of rather opaque films, which showed spongelike shapes (Figure 6). Remarkably, a hierarchical organization of the surface morphology was built up in this self-assembly process. Whereas hemispherical features existed on a micrometer scale (Figure 6a,b), also explicit structuring was observed in the nanometer regime (Figure 6c). This particular morphology resembles the multiple roughness structure of self-cleaning surfaces, which can be found, for example, in the water-repellent leaves of *Colocasia esculenta* or *Nelumbo nucifera*.[17,18] Accordingly the coated surfaces obtained with Trp-Gly as additive show superhydrophobicity with a contact angle of 165° $\pm$ 5° (Figure 6d).

The employment of arginine (Arg) resulted in the formation of deposits consisting of layers of nanoscale platelets (Figure 7a), resembling the nacreous plate structure in seashells. In the cases of all the before-mentioned amino acids or dipeptides (Figures 1, 2 and 6), the deposits or coatings exhibited the same morphology with or without LBL modification of the silicon substrate. From reaction solutions containing glycyl-glutamic acid (Gly-Glu), however, ribbon-like morphologies were found (Figure 7b) on LBL-modified subtrates, whereas no significant deposition occurred on unmodified surface-oxidized silicon (Figure 7c). This is the only, yet most interesting, example in this work where a difference between LBL-modified and unmodified substrates was found.

Further characterization of the deposition products obtained from the reaction solutions containing Trp-Gly, Arg, and Gly-Glu was carried out by means of XRD measurements (Figure

(15) Kistenmacher, T. J. *Acta Crystallogr., B* **1972**, *28*, 1302.
(16) Mar, L. G.; Timbrell, P. Y.; Lamb, R. N. *Thin Solid Films* **1993**, *223*, 341.
(17) Barthlott, W.; Neinhuis, C. *Planta* **1997**, *202*, 1.
(18) Patankar, N. A. *Langmuir* **2004**, *20*, 8209.

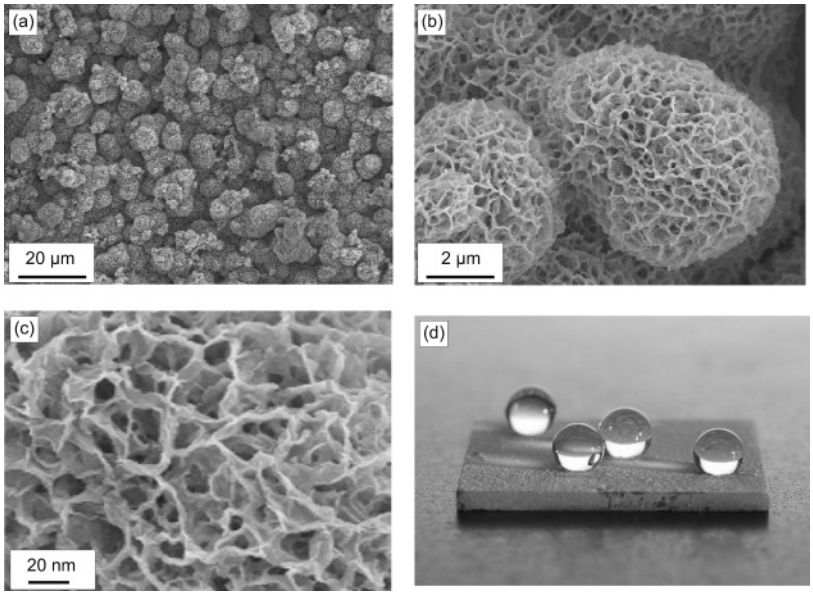

Figure 6. (a)−(c) SEM micrographs of deposition products grown on polyelectrolyte multilayers from solutions containing 30 mM [Zn], 30 mM HMTA, and 7.5 mM Trp-Gly for 48 h at 333 K. The different magnifications reveal the hierarchical structure of the film. (d) Water droplets on the coated substrate (1×1 cm^2).

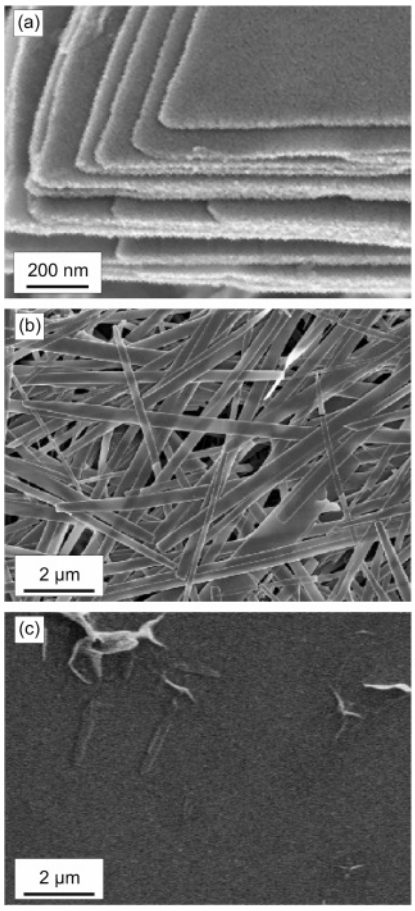

Figure 7. SEM micrographs of deposition products grown on polyelectrolyte multilayers from solutions containing (a) 30 mM [Zn], 30 mM HMTA, and 3.75 mM Arg and (b) 15 mM [Zn], 15 mM HMTA, and 1.88 mM Gly-Glu as well as (c) on surface oxidized silicon from solutions of 15 mM [Zn], 15 mM HMTA, and 1.88 mM Gly-Glu. All samples were grown for 48 h at 333 K.

8). The X-ray patterns had features typical of incompletely ordered lamellar compounds related to the brucite structure, which revealed the presence of layered basic zinc salts (LBZs). LBZs possess a specific layered structure that could

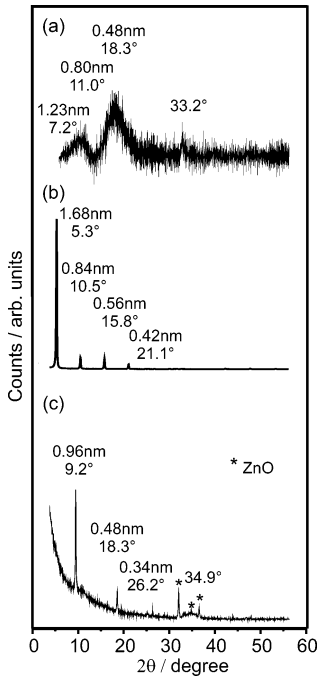

Figure 8. XRD diagrams of deposition products from solutions of (a) 15 mM [Zn], 15 mM HMTA, and 1.88 mM Gly-Glu; (b) 30 mM [Zn], 30 mM HMTA, and 7.5 mM Trp-Gly; and (c) 30 mM [Zn], 30 mM HMTA, and 3.75 mM Arg.

be determined by structure analysis of $Zn_5(OH)_8A_2 \cdot nH_2O$ for A = Cl^- [19] and NO_3^- [19] or $Zn_5(OH)_6(CO_3)_2$.[20] The structure is best described in terms of $[(Zn_{octa})_3(Zn_{tetra})_2(OH)_8]^{2+} \cdot 2(A^-) \cdot nH_2O$ and consists of infinite brucite layers, where one-fourth of the zinc atoms in the octahedral interstices are omitted. On both sides of the empty octahedra Zn atoms are located that are tetrahedrally coordinated. Thus the ratio of octahedral to tetrahedral zinc is 3:2. In the case of the monovalent anions A, the tetrahedral zinc sites are coordinated by three OH^- ions of the brucite layers. The

(19) Allmann, R. *Z. Kristallogr.* **1968**, *126*, 417.
(20) Stählin, W.; Oswald, H. R. *Acta Crystallogr., B* **1970**, *B26*, 860.

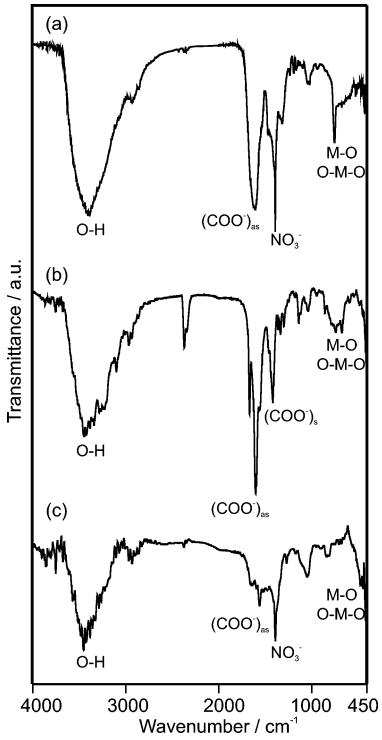

Figure 9. IR spectra of deposition products from solutions of (a) 30 mM [Zn], 30 mM HMTA, and 7.5 mM Trp-Gly; (b) 15 mM [Zn], 15 mM HMTA, and 1.88 mM Gly-Glu; and (c) 30 mM [Zn], 30 mM HMTA, and 3.75 mM Arg.

Table 3. Positions of Symmetric and Asymmetric C═O Stretching Vibrations of Deposition Products from Solutions of (a) 30 mM [Zn], 30 mM HMTA, and 7.5 mM Trp-Gly; (b) 15 mM [Zn], 15 mM HMTA, and 1.88 mM Gly-Glu; and (c) 30 mM [Zn], 30 mM HMTA, and 3.75 mM Arg

additive	ν_{as}(C═O)	ν_{s}(C═O)	ν_{as}(NO_3^-)
(a) Trp-Gly	1599	1411 (sh)	1386
(b) Gly-Glu	1594	1409	
(c) Arg	1595	1410 (sh)	1383

fourth apex of these coordination tetrahedra point into the interlayer space and can then be occupied either by the anion (for Cl^- or CO_3^{2-}) or by a water molecule, whereby the anion is freely situated in the interlayer (in the case of NO_3^-).[19−21]

Whereas the before-mentioned LBZs comprise ordered stacking of the brucite layers, the intercalation of carboxylate anions leads to turbostratic disorder as in the case of basic zinc acetate.[22,23] The resulting diffraction pattern consists of sharp reflections in the range of small diffraction angles and broad asymmetric peaks at high angles.[22] These reflections correspond to the (00*l*) and (*hk*0) peaks, respectively, as all of the mixed (*hkl*) peaks are suppressed completely by the randomness in translation and rotation.[24]

In the present study the overall crystal structure could be indexed in the hexagonal system corresponding to the procedure for basic zinc acetate.[25,26] Accordingly, the peaks

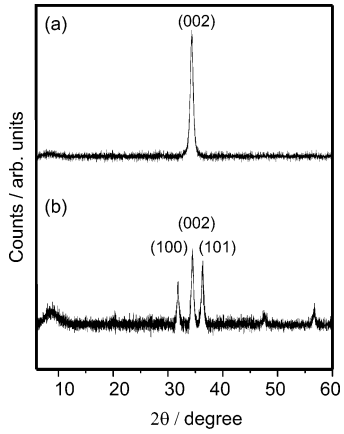

Figure 10. XRD diagrams of deposition products after calcinations at 723 K for 4 h in air of films from solutions of (a) 15 mM [Zn], 15 mM HMTA, and 1.88 mM Gly-Glu and (b) 30 mM [Zn], 30 mM HMTA, and 7.5 mM Trp-Gly.

at the lowest diffraction angles corresponded to the (00*l*) reflections. Thereby the crystal lattice plane distance of the (001) reflection was commonly attributed to the interlamellar distance in the LBZ structure. The values of 1.68 (Gly-Glu) and 1.23 nm (Trp-Gly) were comparable to the corresponding distance in basic zinc acetate,[25] which varied from 1.31 to 1.43 nm depending on the conditions of the synthesis, whereas the value for 0.96 nm (Arg) was slightly smaller.

These findings can also be compared to interlayer bonding of amino acids in layered double hydroxides (LDHs). In LDHs di- and trivalent cations occupy the octahedral sites of brucite layers, between which various types of anions can be situated.[26,27] Rather low interlayer distances were interpreted in the way that the amino acids adopted orientations, in which the longest molecule chords were approximately parallel to the inorganic layers.[27,28]

The rather broad peaks at diffraction angles above 33.2° (Trp-Gly) or 34.9° (Arg), respectively, were assigned to the (*hk*0) reflections. Such peaks were not observed in the case of Gly-Glu, which indicated oriented growth of the deposition product on the substrate. Weak diffraction peaks of zincite in Figure 8c corresponded to minor amounts of co-deposited micrometer-size crystals with morphologies as shown in Figure 1.

The LBZs obtained from the reaction solutions of Trp-Gly, Arg, and Gly-Glu were also characterized by IR spectroscopy (Figure 9). The spectra exhibit the typical bands for carboxylate functions, i.e., the ν_{as} and the ν_{s} stretching modes, which demonstrate the presence of the amino acids or dipeptides (Table 3). The deposition products of solutions containing Trp-Gly and Arg further show a sharp peak at 1385 cm^{-1}, which is characteristic for nitrate anions (Figure 9a,c).[23] This signal, however, does not appear in samples from solutions with Gly-Glu (Figure 9b). The insertion of nitrate was also reported for the above-mentioned LDH compounds, which shows the flexibility of this structure concerning storage and ion exchange properties.[26] The amount of nitrate with respect to the organic anions in the

(21) Ghose, S. *Acta Crystallogr.* **1964**, *17*, 1051.
(22) Poul, L.; Jouini, N.; Fiévet, F. *Chem. Mater.* **2000**, *12*, 3123.
(23) Zhang, J.; Zhang, F.; Ren, L.; Evans, D. G.; Duan, X. *Mater. Chem. Phys.* **2004**, *85*, 207.
(24) Yang, D.; Frindt, R. F. *J. Mater. Res.* **1996**, *11*, 1733.
(25) Hosono, E.; Fujihara, S.; Kimura, T.; Imai, H. *J. Colloid Interface Sci.* **2004**, *272*, 391.
(26) Aisawa, S.; Takahashi, S.; Ogasawara, W.; Umetsu, Y.; Narita, E. *J. Solid State Chem.* **2001**, *162*, 52.
(27) Hibino, T. *Chem. Mater.* **2004**, *16*, 5482.
(28) Newman, S. P.; Di Cristina, T.; Coveney, P..V.; Jones, W. *Langmuir* **2002**, *18*, 2933.

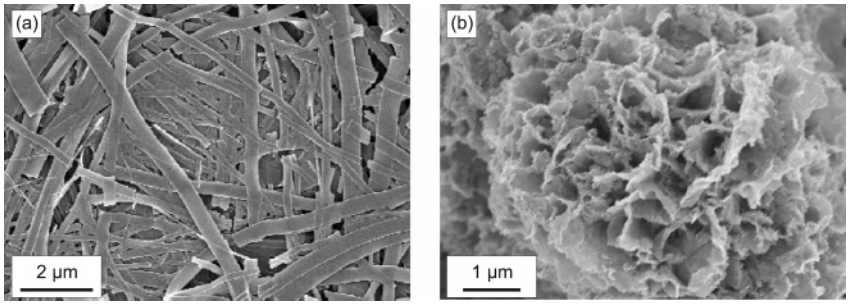

Figure 11. SEM micrographs of deposition products after calcinations at 723 K for 4 h in air. As-deposited materials were obtained after 48 h at 333 K from solutions of (a) 15 mM [Zn], 15 mM HMTA, and 1.88 mM Gly-Glu and (b) 30 mM [Zn], 30 mM HMTA, and 7.5 mM Trp-Gly.

interlayer space was correlated to the charge density of the organic molecules. Thereby amino acids or dipeptides with anionic side groups are more easily intercalated than those with apolar or cationic functions.[26] Correspondingly, Gly-Glu is preferably intercalated compared to Trp-Gly and Arg.

After oxidative calcination of the deposition products, only ZnO remained (Figure 10). Thereafter films from solutions of Gly-Glu revealed an explicit texture, as only the (002) reflection of the zincite structure was present in the XRD digrams (Figure 10a). Here the *c*-axis of the crystallites runs normal to the substrate surface. As mentioned above, the LBZ material derived from Gly-Glu exhibited already preferential orientation to the substrate, which then might have induced oriented growth of zincite in the calcination process. Films from solutions of Trp-Gly exhibit further reflections of zincite after calcination, thus revealing a rather statistical orientation of the crystallites within the film (Figure 10b).

The distinct morphologies, though, were maintained after annealing (Figure 11). This is in agreement with investigations concerning the calcination of films on glass slides of basic zinc acetates with the above-mentioned LBZ structure, which kept a nestlike morphology after heating. The ZnO films obtained in this way did not show preferential orientation with respect to the substrate.[29]

For the formation of coatings or deposits by the CBD process, two mechanisms are discussed in the literature, whereby mixed pathways are of course also imaginable. The first route describes the deposition in terms of formation of colloids in the reaction solution (homogeneous nucleation) and their subsequent attachment on the substrate, which can be understood in terms of the DLVO (Derjaguin, Landau, Verwey, and Overbeck) theory. Alternatively, the successive attachment of ions to the surface (heterogeneous nucleation) can lead to the growth of the coating.[3,4]

In the investigations presented here an important influence of the substrate was revealed for depositions from solutions containing Gly-Glu. In this case the oriented growth of the LBZ on the substrate is observed, which is commonly associated with heterogeneous nucleation.[3] In contrast, the films grown using His as additives seemed to have formed by the attachment of spherical colloidal particles from the solution. To confirm this finding, zeta-potential measurements were carried out. In accordance with the DLVO theory, favorable electrostatic interactions exist with both LBL-modified and unmodified silicon, which both show a negative surface charge at the pH value of the reaction (van der Waals interactions between the particles then contribute to proceeding film growth).[3,12]

Table 4. Morphological Overview

Additive	Structural Formula	Morphology of Deposit	Deposition Product
Cit		micrometer sized crystals	Zinc oxide
Pro		micrometer sized crystals	Zinc oxide
Gly-Gln	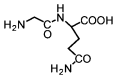	micrometer sized crystals	Zinc oxide
His		uniform film	Zinc oxide
Gly-His	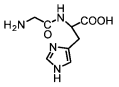	uniform film	Zinc oxide
Trp-Gly	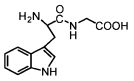	sponge-like coating	LBZ
Gly-Glu	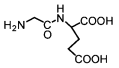	ribbon-like coating	LBZ
Arg		nanoscalic plateles	LBZ

Conclusions

Amino acids and peptides provide a strong influence on the morphology of the deposition products formed during mineralization within aqueous zinc salt solutions (Table 4). The employment of Pro, Cit, and Gly-Gln yielded micron-size zincite crystals. This was similar to the mineralization behavior of ZnO in aqueous solutions of zinc salts and thus indicated a rather weak interaction of these biomolecules with ZnO. His or the peptide Gly-His, though, provided functionalities, which suppressed the formation of larger crystals and stabilized nanosize product particles. This led to the formation of smooth and uniform thin films. The formation of compounds rather than ZnO was observed in the presence

(29) Morioka, H.; Tagaya, H.; Kadokawa, J. I.; Chiba, K. *J. Mater. Sci. Lett.* **1999**, *18*, 995.

of the amino acid Arg as well as the peptides Gly-Glu and Trp-Gly. In these cases sheetlike structures that consisted of layered basic zinc salts were formed. The morphologies resembled the architecture of biomaterials such as the nacreous plate structure in seashells or the surface of water-repellent leaves of plants. Accordingly, the properties of such biomaterials, such as superhydrophobicity, could be mimicked by these synthesized counterparts.

Acknowledgment. This project was supported by the KSB foundation. The help of Dr. P. Lamparter, Dr. S. Wildhack, and Mr. H. Labitzke with the XRD, zeta-potential and SEM measurements, respectively, is gratefully acknowledged. This paper is dedicated to Professor Wolfgang Laqua on the occasion of his 70th birthday.

CM051542O